# Interlayer charge transfer in $ReS_2/WS_2$ van der Waals heterostructures

Peymon Zereshki,[1] Peng Yao,[2] Dawei He,[2] Yongsheng Wang,[2,*] and Hui Zhao[1,†]
[1]*Department of Physics and Astronomy, The University of Kansas, Lawrence, Kansas 66045, USA*
[2]*Key Laboratory of Luminescence and Optical Information, Ministry of Education, Institute of Optoelectronic Technology, Beijing Jiaotong University, Beijing 100044, China*

(Received 15 January 2019; revised manuscript received 8 May 2019; published 21 May 2019)

We observed ultrafast charge transfer between distorted 1*T*-$ReS_2$ with anisotropic in-plane electronic and optical properties and 2*H*-$WS_2$ that is in-plane isotropic. Heterostructures of monolayer $ReS_2$/monolayer $WS_2$ and bilayer $ReS_2$/monolayer $WS_2$ were fabricated by mechanical exfoliation and dry transfer techniques. Significant photoluminescence quenching of $WS_2$ in the heterostructures indicates efficient charge transfer. In femtosecond transient absorption measurements, it was found that holes injected in monolayer or bilayer $ReS_2$ transfer to $WS_2$ on a timescale that is shorter than the time resolution of the measurement. This observation provides evidence that the holes are delocalized in bilayer $ReS_2$, revealing strong van der Waals interlayer couplings. These results also show that $ReS_2$ and $WS_2$ form type-II heterostructures with excellent charge transfer properties.

DOI: 10.1103/PhysRevB.99.195438

## I. INTRODUCTION

Since 2010, two-dimensional (2D) transition-metal dichalcogenides (TMDs) have been a focus of material research due to their interesting electronic, optical, and spin properties [1–3]. Although most initial efforts have been devoted to a few materials, namely, $MoS_2$, $WS_2$, $MoSe_2$, and $WSe_2$ [4], other members of the TMD family have gained significant momentum recently, especially those possessing different and complementary properties. Rhenium disulfide is such a member with several interesting properties. Unlike most TMDs with stable hexagonal phases, $ReS_2$ forms a distorted 1*T* structure with triclinic symmetry [5–7]. The lower lattice symmetry gives rise to in-plane anisotropic lattice, electronic, and optical properties, which have been confirmed by optical [8–12] and transport measurements [13–15]. In addition to the exfoliation method used in early studies, techniques to synthesize large-area and high-quality $ReS_2$ monolayer or thin films have been developed, such as epitaxy [16,17] and chemical vapor deposition [18,19]. The application of $ReS_2$ in various devices, such as transistors [20–24], logic gates [21], and polarization-sensitive photodetectors [20,22,25] has also been explored.

Despite this progress, some of the fundamental issues of this elusive material are still under debate. The most pressing ones include the nature of the lowest band gap and the strength of the interlayer coupling. On the band gap, early studies have indicated that bulk $ReS_2$ has a direct band gap of about 1.5 eV at room temperature [5,26–29]. However, an indirect band gap of 1.47 eV has been reported [30]. Low photoluminescence (PL) quantum yield generally observed in all thicknesses appears to suggest that $ReS_2$ is an indirect semiconductor [31], while *k*-space photoemission microscopy revealed a direct band gap in the bilayer (2L) $ReS_2$ [32]. On the second issue, early experimental and first-principle studies have suggested that the interlayer coupling in $ReS_2$ is much weaker than other TMDs [5]. This suggests that the adjacent 1L's in bulk $ReS_2$ are largely electronically decoupled with the electrons localized in each layer. The extremely weak van der Waals coupling in vertical $ReS_2$ nanowalls was recently utilized for high-current-density Li-ion batteries [33]. However, several evidences were later reported that suggest rather strong interlayer coupling. First, optical absorption and PL measurements showed that the room-temperature optical band gap evolves gradually from 1.47 eV in bulk to 1.61 eV in 1L [10]. Second, interlayer phonon modes were observed in Raman measurements, indicating that the $ReS_2$ layers are coupled and orderly stacked [34,35]. The interlayer force constants were about 55–90% of those of multilayer $MoS_2$ [36]. Third, photoemission microscopic measurements showed that the valence electrons in bulk $ReS_2$ are delocalized across the layers and the valence-band dispersion evolves with the thickness [32]. In addition, qualitatively different charge transport characteristics between 1L and multilayers [37] appear to suggest thickness-dependent band structures.

Here we report direct evidence of electron interlayer delocalization in 2L $ReS_2$ by comparing charge transfer in 1L-$ReS_2$/1L-$WS_2$ and 2L-$ReS_2$/1L-$WS_2$ heterostructures fabricated by mechanical exfoliation and dry transfer. Interlayer charge transfer between 2D materials [38–44] plays a key role in forming 2D heterostructures with emergent properties. Therefore, the study of charge transfer between $ReS_2$ and other TMDs is an important step towards introducing $ReS_2$ to the material library for constructing 2D heterostructures. Interestingly, recent studies have revealed that $ReS_2$ can form type-I band alignment with $MoS_2$ [45], type-II band alignment with $WSe_2$ [46], and type-III broken-gap alignment

*yshwang@bjtu.edu.cn
†huizhao@ku.edu

 

with black phosphorus [47], illustrating the flexibility that band-alignment design $ReS_2$ can provide. However, despite the recent progress in their growth [48] and in device applications [46,49], the charge transfer process in $ReS_2$-based heterostructures is yet to be extensively studied. In this study, by transient absorption and steady-state PL measurements, we found that holes optically injected in $ReS_2$ transfer to $WS_2$ on a sub-100-fs timescale, and the transfer from 2L $ReS_2$ appears to be even faster. This observation suggests that the holes in 2L $ReS_2$ are not localized in each $ReS_2$ layer and thus provide direct evidence of electronic delocalization in this material. Furthermore, the ultrafast charge transfer between $ReS_2$ and $WS_2$ is encouraging news for developing van der Waals heterostructures using $ReS_2$.

## II. SAMPLE FABRICATION AND PHOTOLUMINESCENCE

Figure 1(a) shows the fabricated sample. First, a $ReS_2$ flake containing 1L and 2L regions was mechanically exfoliated on a polydimethylsiloxane (PDMS) substrate. Since the substrate (about 1 mm) is much thicker than the $ReS_2$ flake and is transparent, the optical contrast of the flake is proportional to its thickness [11,51–54]. By investigating a large number of thin flakes, we establish that the contrast of 1L is about 15.5%. Next, the selected $ReS_2$ flake was transferred to a $Si/SiO_2$ (90 nm) substrate. A 1L $WS_2$, fabricated and identified with the same procedure, was then transferred on top of the $ReS_2$ flake such that it covers parts of both 1L and 2L $ReS_2$ regions as well as the substrate. Hence, the same sample contains heterostructure regions of 1L-$ReS_2$/1L-$WS_2$ and 2L-$ReS_2$/1L-$WS_2$, as well as a 1L $WS_2$ region. The sample was annealed for 4 hours at 200 °C under 100 sccm of Ar gas environment with a pressure of 2–3 Torr. All measurements were done at room temperature with the sample under ambient conditions.

The expected band alignment of the 1L-$ReS_2$/1L-$WS_2$ heterostructure is shown in Fig. 1(b). The values shown are adopted from a theoretical study [50]. The conduction-band minimum (CBM) and the valence-band maximum (VBM) are located in the $ReS_2$ and $WS_2$ layers, respectively. Such a type-II band alignment allow charge transfer, i.e., electron transfer from $WS_2$ to $ReS_2$ and hole transfer along the opposite direction. Since the offsets in the conduction and valence bands of 0.58 and 0.37 eV are much larger than the room-temperature lattice thermal energy of 0.025 eV, thermal excitation is unlikely to affect the direction of charge transfer. We note that although other theoretical works have yielded slightly different values of the band offsets, the type-II nature of the alignment has been consistently produced [32,45,55,56].

Figure 1(c) shows the PL spectra from regions of 1L $WS_2$ (blue), 1L-$ReS_2$/1L-$WS_2$ (red), and 2L-$ReS_2$/1L-$WS_2$ (purple), respectively. The measurement was performed with a 405 nm continuous-wave laser with 200 nW power and a focused spot size of about 2 $\mu$m. The spectrum of 1L $WS_2$ peaks at 2.025 eV. The position, quantum yield, and spectral width of this peak are all in good agreement with previous reported values [40,57,58]. The peak shifts to 2.023 eV in the 1L-$ReS_2$/1L-$WS_2$ heterostructure. The reduction of the optical band gap of 2 meV can be attributed to the changes of both the band gap and the exciton binding energy of $WS_2$ caused by the screening effect of $ReS_2$ [40]. The peak further shifts to 2.021 eV in the 2L-$ReS_2$/1L-$WS_2$ heterostructure, which is consistent with the expected larger screening effect due to the doubled thickness. Furthermore, significant quenching of PL was observed in both heterostructures, suggesting efficient charge or energy transfer from $WS_2$ to $ReS_2$ on a timescale shorter than the exciton lifetime in $WS_2$. We moved the laser spot on each heterostructure region and confirmed that the quenching factors of about 15 and 700 in the two regions are reproducible.

It is interesting to note that the spectrum of the 2L-$ReS_2$/1L-$WS_2$ heterostructure has a shoulder at the low-energy side. Since this shoulder is about 100 meV below the main peak, which is close to the trion binding energy of $WS_2$, we attribute this peak to trions, which is confirmed by the dependence of the PL spectrum on the excitation power (see the Supplemental Material [59]). We note that this shoulder is also visible in the 1L-$ReS_2$/1L-$WS_2$ region, although it is less pronounced.

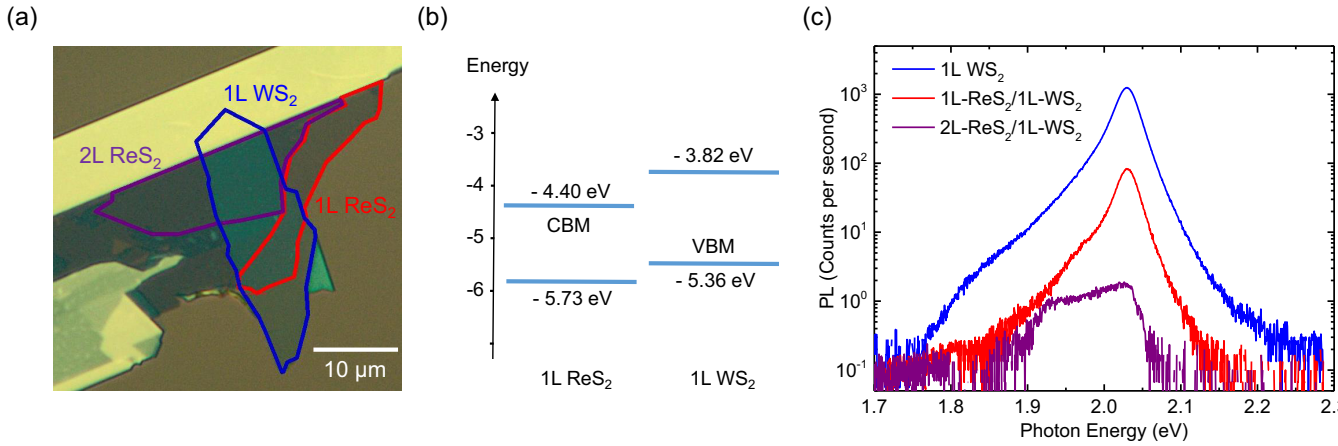


FIG. 1. (a) An optical microscopy image of the sample. (b) Band alignment of 1L-$ReS_2$/1L-$WS_2$ according to theory [50]. (c) PL of 1L $WS_2$ (blue), 1L-$ReS_2$/1L-$WS_2$ (red), and 2L-$ReS_2$/1L-$WS_2$ (purple).

TABLE I. Summary of the time constants deduced from the exponential fits.

| Sample | $\tau_1$ (weight) | $\tau_2$ (weight) | $\tau_3$ (weight) | Background |
|---|---|---|---|---|
| 1L $WS_2$ | $1.9 \pm 0.3$ ps (31%) | $22 \pm 3$ ps (39%) | $115 \pm 30$ ps (21%) | 9% |
| 1L $ReS_2$ | $3.6 \pm 0.6$ ps (33%) | $160 \pm 20$ ps (60%) | (0%) | 7% |
| 2L $ReS_2$ | $4.1 \pm 0.4$ ps (45%) | $117 \pm 15$ ps (55%) | (0%) | 0% |
| 1L-$ReS_2$/1L-$WS_2$ | $1.3 \pm 0.2$ ps (15%) | $330 \pm 50$ ps (7%) | (0%) | 78% |
| 2L $ReS_2$/1L-$WS_2$ | $1.0 \pm 0.2$ ps (50%) | $46 \pm 5$ ps (14%) | (0%) | 36% |

## III. TIME-RESOLVED MEASUREMENTS

Charge carrier dynamics was studied by transient absorption measurements in the reflection geometry. In the experimental setup, a Ti:sapphire laser generates 100 fs pulses with a central wavelength of about 780–790 nm, a spectral width of about 10 nm, and a repetition rate of 80 MHz. One part of this beam is sent to a nonlinear optical crystal to generate second harmonic pulses of about 390–395 nm. The rest of the beam is used to pump an optical parametric oscillator to produce a near-infrared pulse in the range of 1220–1280 nm, where the second harmonic in the range of 610–640 nm is close to the optical band gap of $WS_2$. The output of the Ti:sapphire can also be used directly in the experiment. In a certain experimental configuration, two of these pulses are used as the pump and probe, which are combined by a beam splitter and are focused to the sample from the normal direction through a microscope objective lens. The reflected probe beam is sent to a photodetector, with the output measured by a lock-in amplifier. The intensity of the pump beam is modulated by a mechanical chopper at about 3 KHz. With the configuration, the lock-in amplifier measured the differential reflection of the probe as the probe delay (defined as the arrival time of the probe pulse at the sample with respect to the pump pulse) was varied by changing the probe path length. The differential reflection is defined as $\Delta R/R_0 = (R - R_0)/R_0$, where $R$ and $R_0$ are the probe reflectance with and without the presence of the pump beam, respectively.

We first studied the photocarrier dynamics in individual 1L $WS_2$, 1L $ReS_2$, and 2L $ReS_2$ regions. For 1L $WS_2$, a 3.18 eV pump pulse with an energy fluence of 3 $\mu$J cm$^{-2}$ was used to inject free carriers. Using an absorption coefficient of $7.5 \times 10^7$ m$^{-1}$ [60], the estimated peak density of injected electron-hole pairs is about $3 \times 10^{11}$ cm$^{-2}$. The differential reflection measured with a 2.01 eV probe pulse, which is near the optical band gap of $WS_2$, is shown by the blue squares in Fig. 2 for short-time [Fig. 2(a)] and long-time [Fig. 2(b)] ranges, respectively. The rise of the signal can be fit by the integral of a Gaussian function with a full width at half maximum of 0.375 ps, as indicated by the curve in Fig. 2(a). This time is longer than the cross correlation of the pump and probe pulses of about 200 fs, which suggests that the injected free carriers produce a maximum signal at the exciton resonance at a slightly delayed time. The decay of the signal can be fit by a triexponential function, $\Delta R/R_0(t) = A_1\exp(-t/\tau_1) + A_2\exp(-t/\tau_2) + A_3\exp(-t/\tau_3) + B$, as shown by the blue curve in Fig. 2(b), with the three processes of time constants (and weights) of $\tau_1$ of $1.9 \pm 0.3$ ps (31%), $\tau_2$ of $22 \pm 3$ ps (39%), $\tau_3$ of $115 \pm 30$ ps (21%), and a background of 9%. Based on previous studies, the $\tau_1$ process can be related to the formation of excitons from free carriers [61,62], which causes reduction of the signal. However, we note that the time constant observed from this sample is longer than previous studies [61,62]. We attribute the 22 ps process to exciton recombination, which is consistent with the previously reported exciton lifetime in 1L $WS_2$ [63]. The rest of the process, which accounts for about 30% of the signal, could be attributed to effects of lattice heating by the laser pulse or defects. All of the time constants are summarized in Table I for better comparison, along with those from the heterostructures.

The magenta and black symbols in Fig. 2 show the signal from the 1L and 2L $ReS_2$ regions, respectively. For clarity, both signals have been multiplied by a factor of 5. In these measurements, the same pump photon energy (3.18 eV) and fluence (3 $\mu$J cm$^{-2}$) were used, while the probe was tuned to 1.61 eV, which is about 0.1 eV above the optical band gap of $ReS_2$. With an absorption coefficient of $3.5 \times 10^7$ m$^{-1}$, [26] the pump injects a peak carrier density of $1.35 \times 10^{11}$ and $2.7 \times 10^{11}$ cm$^{-2}$ in the 1L and 2L $ReS_2$ regions, respectively. From Fig. 2(a), the signals show a slower rise, compared to $WS_2$, of about less than 1 ps. Since the pump photon energy is much larger than the band gap of $ReS_2$, the rise could be attributed to energy relaxation of the hot carriers from their injected states to the states that are probed. The decay of the signal in both regions can be fit by a biexponential

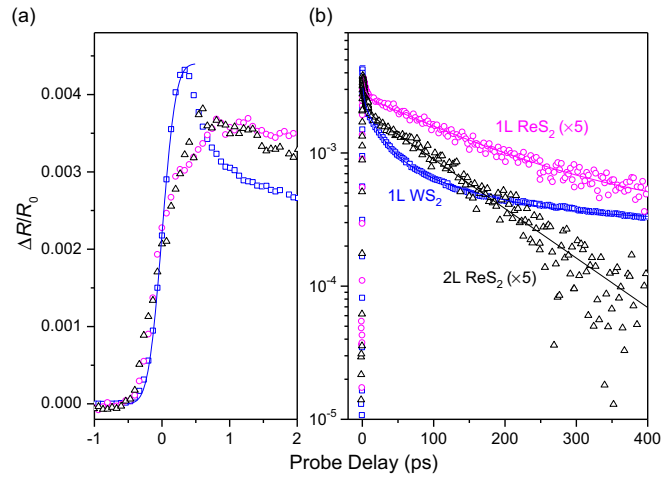


FIG. 2. Differential reflection of individual materials of 1L $WS_2$ (blue squares), 1L $ReS_2$ (magenta circles), and 2L $ReS_2$ (black triangles) over (a) short- and (b) long-time ranges. Photocarriers are injected by a 3.18 eV pump and detected by probes of 2.01 eV for $WS_2$ and 1.61 eV for both $ReS_2$ regions, respectively. The curves are fits (see text).

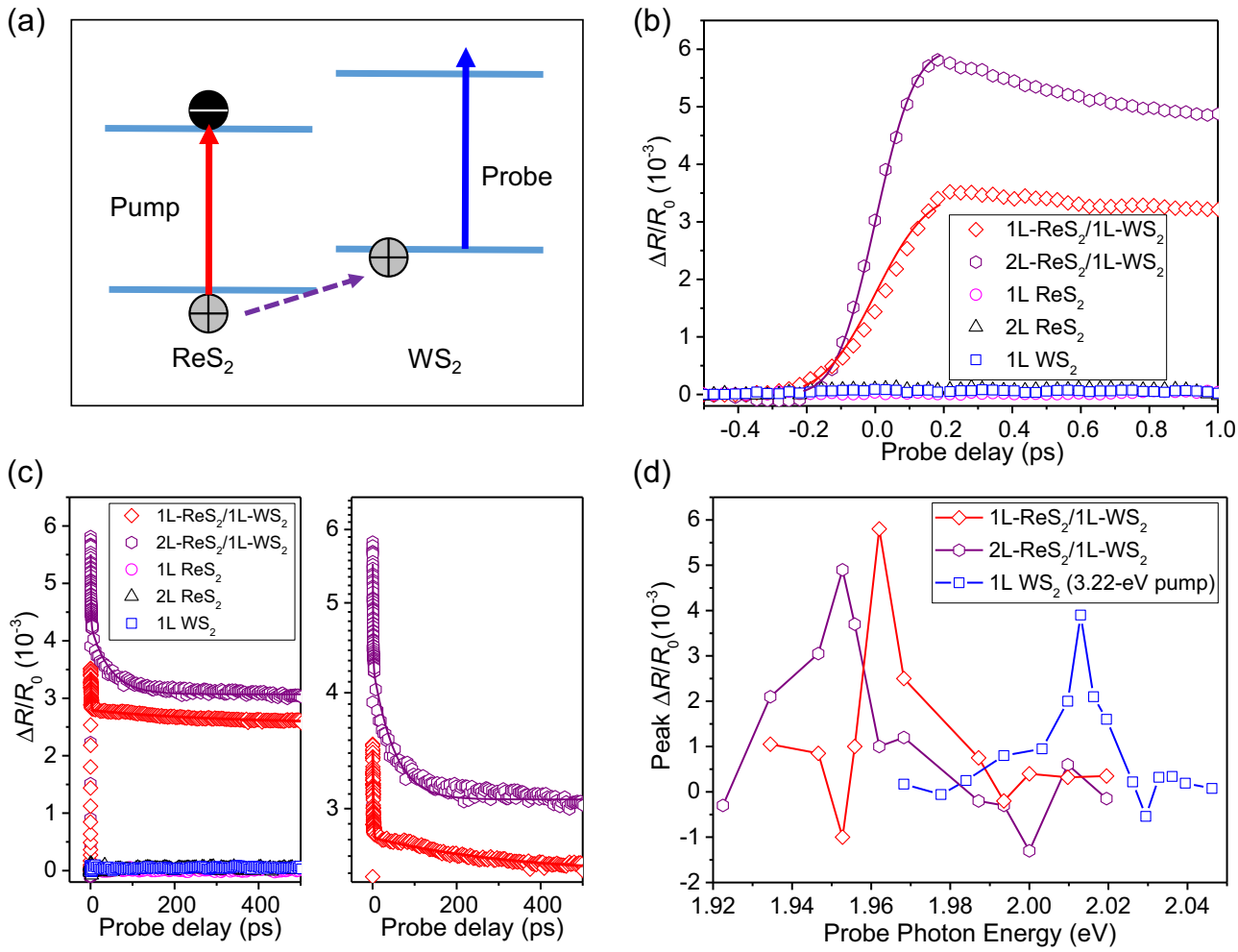


FIG. 3. (a) Schematics of the pump-probe configuration to study hole transfer from $ReS_2$ to $WS_2$. (b) Differential reflection signal obtained from the heterostructures of 1L-$ReS_2$/1L-$WS_2$ (red diamonds) and 2L-$ReS_2$/1L-$WS_2$ (purple hexagons) using the configuration shown in (a). Results of the same measurements on regions of 1L $WS_2$ (blue squares), 1L $ReS_2$ (magenta circles), and 2L $ReS_2$ (black triangles) are also shown for comparison. (c) Same as (b), but with a longer-time range and with linear (left) and logarithmic scales. (d) Peak differential reflection signal as a function of the probe photon energy for the two heterostructures and the 1L $WS_2$.

function, $\Delta R/R_0(t) = A_1\exp(-t/\tau_1) + A_2\exp(-t/\tau_2) + B$. For the 1L, the two time constants are $\tau_1 = 3.6 \pm 0.6$ ps (33%) and $\tau_2 = 160 \pm 20$ ps (60%), with a background of 7% (magenta curve). For the 2L, these parameters are $\tau_1 = 4.1 \pm 0.4$ ps (45%) and $\tau_2 = 117 \pm 15$ ps (55%), with almost no background (black curve). Both the magnitude and the time evolution of the signal from the two $ReS_2$ regions are similar, suggesting similar carrier dynamics in 1L and 2L $ReS_2$. The long-time constants can be attributed to the exciton lifetime in these samples.

With the information on carrier dynamics in the three individual materials, we next studied charge transfer between them. To probe potential hole transfer from $ReS_2$ to $WS_2$, we used the configuration shown in Fig. 3(a). A 1.57 eV pump pulse selectively excites carriers in 1L or 2L $ReS_2$. Since the photon energy is smaller than its optical band gap, the $WS_2$ layer is not excited. If the VBM of $ReS_2$ is lower than $WS_2$, as theoretically predicted, holes are expected to transfer to $WS_2$ to lower their potential energy. By using a probe tuned near the optical band gap of $WS_2$, we monitor the appearance of these holes in $WS_2$ and time resolve their dynamics. Electrons are expected to reside in $ReS_2$, which has the lower CBM. The separation of the electrons and holes is expected to allow the formation of spatially indirect excitons with prolonged lifetime [64,65].

The differential reflection signals obtained with this configuration from the 1L-$ReS_2$/1L-$WS_2$ and 2L-$ReS_2$/1L-$WS_2$ heterostructures are shown by the red diamonds and purple hexagons in Figs. 3(b) and 3(c) for short- and long-time ranges, respectively. In these measurements, the pump injects carrier densities of $4.1 \times 10^{11}$ and $8.2 \times 10^{11}$ $cm^{-2}$ in 1L and 2L $ReS_2$, respectively. The probe photon energies used are 1.97 and 1.95 eV for 1L-$Re_2$/1L-$WS_2$ and 2L-$ReS_2$/1L-$WS_2$ heterostructures, respectively. The rather strong signal suggests the occurrence of hole transfer. We next studied the dependence of the signal magnitude on the probe photon energy for the two heterostructure samples. As shown in Fig. 3(d), both heterostructures show a pronounced resonant feature near the A-exciton of $WS_2$ that is consistent with PL peaks shown in Fig. 1(c). For comparison, probe-photon-

energy dependence of the 1L $WS_2$ sample was also plotted, which was obtained by using a pump pulse of 3.18 eV. These differential reflection spectra show that the signal indeed originates from the change of the excitonic resonance of $WS_2$, instead of from higher-energy states in $ReS_2$. To further confirm the origin of the signal, we repeated the measurement on the three regions of the individual materials. No signal was observed, as shown by the magenta circles (1L $ReS_2$), black triangles (2L $ReS_2$), and blue squares (1L $WS_2$). This is expected since for the 1L $WS_2$ region, the pump does not inject carriers, while for the $ReS_2$ regions, the probe is far away from their optical band gaps and thus has low probing efficiency.

Having established the hole transfer process, we now compare the two heterostructures. First, the red diamonds in Fig. 3(b) show that the signal in 1L-$ReS_2$/1L-$WS_2$ rises to its peak rapidly. The red curve over the data represents the integral of a Gaussian function with a full width at half maximum of 0.28 ps, showing the ultrafast nature of the hole transfer process. Interestingly, for 2L-$ReS_2$/1L-$WS_2$, the rising time corresponds to a width of 0.22 ps, as shown by the purple circles and curve in Fig. 3(b), which suggests that hole transfer from 2L $ReS_2$ to $WS_2$ is faster than from 1L $ReS_2$ to $WS_2$. If the two $ReS_2$ layers are decoupled with holes localized in each layer, one would expect the transfer from 2L to be slower, with an additional transfer step between the two $ReS_2$ layers. Hence, we conclude the two $ReS_2$ layers are coupled and the holes are delocalized.

To analyze the carrier dynamics, we fit the decay process of the signal from the 1L-$ReS_2$/1L-$WS_2$ heterostructure with a biexponential function, $\Delta R/R_0(t) = A_1\exp(-t/\tau_1) + A_2\exp(-t/\tau_2) + B$. The results are plotted in Fig. 3(c) as the red curve over the data, with parameters of $A_1 = 0.5 \times 10^{-3}$, $A_2 = 0.24 \times 10^{-3}$, $B = 2.6 \times 10^{-3}$, $\tau_1 = 1.3 \pm 0.2$ ps, and $\tau_2 = 330 \pm 50$ ps. The fast process of picosecond has been similarly observed in TMD monolayers and was attributed to exciton formation of free electron-hole pairs [61,62], which lowers the effectiveness of carriers in changing the exciton resonance. Here, we assign this process to the formation of interlayer excitons between the transferred holes in $WS_2$ and the electrons in $ReS_2$. The most significant feature observed is the long-lived signal that accounts for a large portion (about 80%) of the total signal. This suggests that indirect excitons formed after holes transfer have a very long lifetime, which is reasonable considering the spatial separation of electrons and holes. This observation further confirms the type-II nature of the band alignment between 1L $ReS_2$ and 1L $WS_2$. We note that such a long-lived and pronounced signal was not observed in the individual materials (see Fig. 2). The intermediate $\tau_2$ process only accounts for a few percent of the signal. This process could be due to various aspects of the dynamics of the indirect excitons following their formation, such as thermalization, energy relaxation, and multiexciton annihilation. More studies are necessary to fully understand this process. However, given that this process makes a minor (7%) contribution to the signal, the uncertainty of its nature does not influence the main conclusion of this study. The signal from 2L-$ReS_2$/1L-$WS_2$ (purple hexagons) is similar to 1L-$ReS_2$/1L-$WS_2$. By using the same biexponential function (purple curve over the data), we find the parameter of $A_1 = 4.4 \times 10^{-3}$, $A_2 = 1.2 \times 10^{-3}$, $B = 3.1 \times 10^{-3}$, $\tau_1 = 1.0 \pm 0.2$ ps, and $\tau_2 = 46 \pm 5$ ps. Similarly, indirect excitons have a very long lifetime. We note that unlike the 1L $WS_2$ sample, no effect from lattice heating was observed here due to the dominate signal from indirect excitons.

## IV. CONCLUSION

We have observed interlayer charge transfer in heterostructures of 1L-$ReS_2$/1L-$WS_2$ and 2L-$ReS_2$/1L-$WS_2$ by femtosecond transient absorption measurements. In the former heterostructure, holes injected in $ReS_2$ transfer to $WS_2$ on an ultrafast timescale, which is encouraging news for incorporating $ReS_2$ to the material library for fabricating van der Waals heterostructures. The hole transfer from 2L $ReS_2$ to $WS_2$ was found to be even faster. If the holes in 2L $ReS_2$ were localized in each layer, the transfer would require an additional step of interlayer transfer within $ReS_2$ and thus would be slower. Hence, this observation is evidence that the holes are delocalized, illustrating the strong interlayer coupling in $ReS_2$. The difference in the charge transfer time could be attributed to the different band structures in 1L and 2L $ReS_2$. These results show that the band alignment of both heterostructures is type II, which is consistent with theoretical predictions.

## ACKNOWLEDGMENTS

We are grateful for the financial support of the National Key R&D Program of China (Grant No. 2016 YFA0202302), the National Natural Science Foundation of China (Grants No. 61527817 and No. 61875236), and National Science Foundation of the USA (Grant No. DMR-1505852).

[1] K. S. Novoselov, A. Mishchenko, A. Carvalho, and A. H. C. Neto, Science **353**, aac9439 (2016).
[2] G. Wang, A. Chernikov, M. M. Glazov, T. F. Heinz, X. Marie, T. Amand, and B. Urbaszek, Rev. Mod. Phys. **90**, 021001 (2018).
[3] S. Manzeli, D. Ovchinnikov, D. Pasquier, O. V. Yazyev, and A. Kis, Nat. Rev. Mater. **2**, 17033 (2017).
[4] Z. Lin, A. McCreary, N. Briggs, S. Subramanian, K. H. Zhang, Y. F. Sun, X. F. Li, N. J. Borys, H. T. Yuan, S. K. Fullerton-Shirey, A. Chernikov, H. Zhao, S. McDonnell, A. M. Lindenberg, K. Xiao, B. J. LeRoy, M. Drndic, J. C. M. Hwang, J. Park, M. Chhowalla, R. E. Schaak, A. Javey, M. C. Hersam, J. Robinson, and M. Terrones, 2D Mater. **3**, 042001 (2016).
[5] S. Tongay, H. Sahin, C. Ko, A. Luce, W. Fan, K. Liu, J. Zhou, Y.-S. Huang, C.-H. Ho, J. Yan, D. F. Ogletree, S. Aloni, J. Ji, S. Li, J. Li, F. M. Peeters, and J. Wu, Nat. Commun. **5**, 3252 (2014).
[6] S. P. Kelty, A. F. Ruppert, R. R. Chianelli, J. Ren, and M. H. Whangbo, J. Am. Chem. Soc. **116**, 7857 (1994).
[7] H. H. Murray, S. P. Kelty, R. R. Chianelli, and C. S. Day, Inorg. Chem. **33**, 4418 (1994).

[8] C. H. Ho, Y. S. Huang, K. K. Tiong, and P. C. Liao, Phys. Rev. B **58**, 16130 (1998).

[9] Q. Cui, J. He, M. Z. Bellus, M. Mirzokarimov, T. Hofmann, H.-Y. Chiu, M. Antonik, D. He, Y. Wang, and H. Zhao, Small **11**, 5565 (2015).

[10] O. B. Aslan, D. A. Chenet, A. M. van der Zande, J. C. Hone, and T. F. Heinz, ACS Photon. **3**, 96 (2016).

[11] Q. Cui, R. A. Muniz, J. E. Sipe, and H. Zhao, Phys. Rev. B **95**, 165406 (2017).

[12] S. S. Zhang, N. N. Mao, N. Zhang, J. X. Wu, L. M. Tong, and J. Zhang, ACS Nano **11**, 10366 (2017).

[13] C. H. Ho, Y. S. Huang, K. K. Tiong, and P. C. Liao, J. Phys. - Condens. Mat. **11**, 5367 (1999).

[14] Y. C. Lin, H. P. Komsa, C. H. Yeh, T. Bjorkman, Z. Y. Liang, C. H. Ho, Y. S. Huang, P. W. Chiu, A. V. Krasheninnikov, and K. Suenaga, ACS Nano **9**, 11249 (2015).

[15] K. Friemelt, M. C. Luxsteiner, and E. Bucher, J. Appl. Phys. **74**, 5266 (1993).

[16] F. F. Cui, C. Wang, X. B. Li, G. Wang, K. Q. Liu, Z. Yang, Q. L. Feng, X. Liang, Z. Y. Zhang, S. Z. Liu, Z. B. Lei, Z. H. Liu, H. Xu, and J. Zhang, Adv. Mater. **28**, 5019 (2016).

[17] X. B. Li, F. F. Cui, Q. L. Feng, G. Wang, X. S. Xu, J. X. Wu, N. N. Mao, X. Liang, Z. Y. Zhang, J. Zhang, and H. Xu, Nanoscale **8**, 18956 (2016).

[18] K. Keyshar, Y. J. Gong, G. L. Ye, G. Brunetto, W. Zhou, D. P. Cole, K. Hackenberg, Y. M. He, L. Machado, M. Kabbani, A. H. C. Hart, B. Li, D. S. Galvao, A. George, R. Vajtai, C. S. Tiwary, and P. M. Ajayan, Adv. Mater. **27**, 4640 (2015).

[19] K. D. Wu, B. Chen, S. J. Yang, G. Wang, W. Kong, H. Cai, T. Aoki, E. Soignard, X. Marie, A. Yano, A. Suslu, B. Urbaszek, and S. Tongay, Nano Lett. **16**, 5888 (2016).

[20] J. Shim, A. Oh, D. H. Kang, S. Oh, S. K. Jang, J. Jeon, M. H. Jeon, M. Kim, C. Choi, J. Lee, S. Lee, G. Y. Yeom, Y. J. Song, and J. H. Park, Adv. Mater. **28**, 6985 (2016).

[21] A. Dathbun, Y. Kim, S. Kim, Y. Yoo, M. S. Kang, C. Lee, and J. H. Cho, Nano Lett. **17**, 2999 (2017).

[22] E. Zhang, Y. B. Jin, X. Yuan, W. Y. Wang, C. Zhang, L. Tang, S. S. Liu, P. Zhou, W. D. Hu, and F. X. Xiu, Adv. Funct. Mater. **25**, 4076 (2015).

[23] E. F. Liu, M. S. Long, J. W. Zeng, W. Luo, Y. J. Wang, Y. M. Pan, W. Zhou, B. G. Wang, W. D. Hu, Z. H. Ni, Y. M. You, X. A. Zhang, S. Q. Qin, Y. Shi, K. Watanabe, T. Taniguchi, H. T. Yuan, H. Y. Hwang, Y. Cui, F. Miao, and D. Y. Xing, Adv. Funct. Mater. **26**, 1938 (2016).

[24] C. M. Corbett, C. McClellan, A. Rai, S. S. Sonde, E. Tutuc, and S. K. Banerjee, ACS Nano **9**, 363 (2015).

[25] F. C. Liu, S. J. Zheng, X. X. He, A. Chaturvedi, J. F. He, W. L. Chow, T. R. Mion, X. L. Wang, J. D. Zhou, Q. D. Fu, H. J. Fan, B. K. Tay, L. Song, R. H. He, C. Kloc, P. M. Ajayan, and Z. Liu, Adv. Funct. Mater. **26**, 1169 (2016).

[26] K. Friemelt, L. Kulikova, L. Kulyuk, A. Siminel, E. Arushanov, C. Kloc, and E. Bucher, J. Appl. Phys. **79**, 9268 (1996).

[27] C. H. Ho, P. C. Liao, Y. S. Huang, and K. K. Tiong, Phys. Rev. B **55**, 15608 (1997).

[28] C. H. Ho, P. C. Liao, Y. S. Huang, and K. K. Tiong, Solid State Commun. **103**, 19 (1997).

[29] C. H. Ho, Y. S. Huang, J. L. Chen, T. E. Dann, and K. K. Tiong, Phys. Rev. B **60**, 15766 (1999).

[30] I. Gutierrez-Lezama, B. A. Reddy, N. Ubrig, and A. F. Morpurgo, 2D Mater. **3**, 045016 (2016).

[31] N. B. Mohamed, K. Shinokita, X. F. Wang, H. E. Lim, D. Z. Tan, Y. Miyauchi, and K. Matsuda, Appl. Phys. Lett. **113**, 121112 (2018).

[32] M. Gehlmann, I. Aguilera, G. Bihlmayer, S. Nemsak, P. Nagler, P. Gospodaric, G. Zamborlini, M. Eschbach, V. Feyer, F. Kronast, E. Mlynczak, T. Korn, L. Plucinski, C. Schuller, S. Blugel, and C. M. Schneider, Nano Lett. **17**, 5187 (2017).

[33] Q. Zhang, S. J. Tan, R. G. Mendes, Z. T. Sun, Y. T. Chen, X. Kong, Y. H. Xue, M. H. Rummeli, X. J. Wu, S. L. Chen, and L. Fu, Adv. Mater. **28**, 2616 (2016).

[34] R. He, J. A. Yan, Z. Y. Yin, Z. P. Ye, G. H. Ye, J. Cheng, J. Li, and C. H. Lui, Nano Lett. **16**, 1404 (2016).

[35] E. Lorchat, G. Froehlicher, and S. Berciaud, ACS Nano **10**, 2752 (2016).

[36] X. F. Qiao, J. B. Wu, L. W. Zhou, J. S. Qiao, W. Shi, T. Chen, X. Zhang, J. Zhang, W. Ji, and P. H. Tan, Nanoscale **8**, 8324 (2016).

[37] D. Ovchinnikov, F. Gargiulo, A. Allain, D. J. Pasquier, D. Dumcenco, C. H. Ho, O. V. Yazyev, and A. Kis, Nat. Commun. **7**, 12391 (2016).

[38] X. Hong, J. Kim, S. F. Shi, Y. Zhang, C. Jin, Y. Sun, S. Tongay, J. Wu, Y. Zhang, and F. Wang, Nat. Nanotechnol. **9**, 682 (2014).

[39] F. Ceballos, M. Z. Bellus, H. Y. Chiu, and H. Zhao, ACS Nano **8**, 12717 (2014).

[40] F. Ceballos, M. Z. Bellus, H. Y. Chiu, and H. Zhao, Nanoscale **7**, 17523 (2015).

[41] B. Peng, G. Yu, X. Liu, B. Liu, X. Liang, L. Bi, L. Deng, T. C. Sum, and K. P. Loh, 2D Mater. **3**, 025020 (2016).

[42] H. M. Zhu, J. Wang, Z. Z. Gong, Y. D. Kim, J. Hone, and X. Y. Zhu, Nano Lett. **17**, 3591 (2017).

[43] L. Yuan, T. F. Chung, A. Kuc, Y. Wan, Y. Xu, Y. P. Chen, T. Heine, and L. B. Huang, Sci. Adv. **4**, e1700324 (2018).

[44] X. W. Wen, H. L. Chen, T. M. Wu, Z. H. Yu, Q. R. Yang, J. W. Deng, Z. T. Liu, X. Guo, J. X. Guan, X. Zhang, Y. J. Gong, J. T. Yuan, Z. H. Zhang, C. Y. Yi, X. F. Guo, P. M. Ajayan, W. Zhuang, Z. R. Liu, J. Lou, and J. R. Zheng, Nat. Commun. **9**, 1859 (2018).

[45] M. Z. Bellus, M. Li, S. Lane, F. Ceballos, Q. Cui, X. C. Zeng, and H. Zhao, Nanoscale Horiz. **2**, 31 (2016).

[46] C. Park, N. T. Duong, S. Bang, D. A. Nguyen, H. M. Oh, and M. S. Jeong, Nanoscale **10**, 20306 (2018).

[47] J. Shim, S. Oh, D. H. Kang, S. H. Jo, M. H. Ali, W. Y. Choi, K. Heo, J. Jeon, S. Lee, M. Kim, Y. J. Song, and J. H. Park, Nat. Commun. **7**, 13413 (2016).

[48] T. Zhang, B. Jiang, Z. Xu, R. G. Mendes, Y. Xiao, L. F. Chen, L. W. Fang, T. Gemming, S. L. Chen, M. H. Rummeli, and L. Fu, Nat. Commun. **7**, 13911 (2016).

[49] B. Kang, Y. Kim, W. J. Yoo, and C. Lee, Small **14**, 1802593 (2018).

[50] V. O. Özcelik, J. G. Azadani, C. Yang, S. J. Koester, and T. Low, Phys. Rev. B **94**, 035125 (2016).

[51] C. Ruppert, O. B. Aslan, and T. F. Heinz, Nano Lett. **14**, 6231 (2014).

[52] F. Ceballos, P. Zereshki, and H. Zhao, Phys. Rev. Mater. **1**, 044001 (2017).

[53] P. Zereshki, Y. Q. Wei, F. Ceballos, M. Z. Bellus, S. D. Lane, S. D. Pan, R. Long, and H. Zhao, Nanoscale **10**, 11307 (2018).

[54] P. Zereshki, Y. Wei, R. Long, and H. Zhao, J. Phys. Chem. Lett. **9**, 5970 (2018).

[55] J. Kang, S. Tongay, J. Zhou, J. B. Li, and J. Q. Wu, Appl. Phys. Lett. **102**, 012111 (2013).

[56] M. Li, M. Z. Bellus, J. Dai, L. Ma, X. L. Li, H. Zhao, and X. C. Zeng, Nanotechnology **29**, 335203 (2018).

[57] N. Peimyoo, W. Yang, J. Shang, X. Shen, Y. Wang, and T. Yu, ACS Nano **8**, 11320 (2014).

[58] Z. Ye, T. Cao, K. O'Brien, H. Zhu, X. Yin, Y. Wang, S. G. Louie, and X. Zhang, Nature (London) **513**, 214 (2014).

[59] See Supplemental Material at http://link.aps.org/supplemental/10.1103/PhysRevB.99.195438 for more data on the identification of the trion peak.

[60] H.-L. Liu, C.-C. Shen, S.-H. Su, C.-L. Hsu, M.-Y. Li, and L.-J. Li, Appl. Phys. Lett. **105**, 201905 (2014).

[61] F. Ceballos, Q. Cui, M. Z. Bellus, and H. Zhao, Nanoscale **8**, 11681 (2016).

[62] P. Steinleitner, P. Merkl, P. Nagler, J. Mornhinweg, C. Schuller, T. Korn, A. Chernikov, and R. Huber, Nano Lett. **17**, 1455 (2017).

[63] C. Mai, Y. G. Semenov, A. Barrette, Y. Yu, Z. Jin, L. Cao, K. W. Kim, and K. Gundogdu, Phys. Rev. B **90**, 041414(R) (2014).

[64] P. Rivera, J. R. Schaibley, A. M. Jones, J. S. Ross, S. Wu, G. Aivazian, P. Klement, K. Seyler, G. Clark, N. J. Ghimire, J. Yan, D. G. Mandrus, W. Yao, and X. Xu, Nat. Commun. **6**, 6242 (2015).

[65] P. Nagler, G. Plechinger, M. V. Ballottin, A. Mitioglu, S. Meier, N. Paradiso, C. Strunk, A. Chernikov, P. C. M. Christianen, C. Schuller, and T. Korn, 2D Mater. **4**, 025112 (2017).